High Coupling Efficiency Silicon Waveguide to Metal–Insulator–Metal Waveguide Mode Converter

Bing Qing Zhu and Hon Ki Tsang, *Senior Member, IEEE*

***Abstract*—Conventional silicon optical waveguides can have efficient coupling to optical fibers using grating couplers, but there is no structure of comparable coupling efficiency, optical bandwidth, and small size for direct coupling from optical fibers to metal slot optical waveguides. In this paper, we propose two structures for efficient coupling from conventional silicon strip waveguide to metal–insulator–metal (MIM) waveguide. The previously reported approach of mode conversion using taper-funnel structures to gradually squeeze the strip mode into metal slot has a big difference in effective indices and a large mismatch between the modes, thus limiting their coupling efficiency. Here, we demonstrate that adding another silicon strip-slot mode converter before the silicon taper structure can improve the coupling efficiency. Furthermore, the reversed taper-funnel structure has lower metallic absorption loss, thus further increasing the coupling efficiency. We experimentally measured 3 dB/coupler loss for coupling to a 200-nm-wide MIM slot, and 4 dB/coupler in the case of coupling to an 80-nm-wide MIM slot at 1640-nm wavelength.**

***Index Terms*—Integrated optics, nanophotonics, optical coupling, plasmonics, subwavelength optical interconnects.**

I. Introduction

With the development of nano-fabrication techniques, nanoscale precision devices can be implemented, which makes the dense integrated photonic circuits possible. But the size of conventional silicon waveguides are still not comparable to electronic ones due to the diffraction limit of light. It is well known that the interface between metal and dielectric can excite and guide surface plasmon-polariton (SPP) modes through the interaction of photon and electron oscillation, and that plasmonic devices can manipulate light far below the diffraction limit [1]. There are three widely used plasmonic waveguide structures, namely, nanoparticle array waveguide, insulator-metal-insulator (IMI) structure and metal-insulator-metal (MIM) structure. Among these, only MIM and nanoparticle array waveguide can support real sub-diffraction modal confinement [2], [3]. The propagation loss in MIM structure is much lower than that in nanoparticle array waveguide due to their completely different excitation principles, that is, propagation SPP in MIM structure and localization SPP in nanoparticle array waveguide [4]. In recent years, MIM waveguide has received considerable attention because of its highly confined nanometer-size mode and lower propagation loss. It has potential for use in future on-chip dense integration of optical and optoelectronic devices, especially for applications of energy efficient high speed optical modulators and interconnects [5], [6].

In order to take good advantage of the highly confined field achieved by MIM waveguide, a low loss coupler between plasmonic structure and other photonic platform is much needed. There are two ways of coupling external light into MIM waveguide and exciting SPPs. One approach is out-of-plane coupling using either a grating coupler [7] or a prism coupler [8] to couple light from free-space into MIM structure. The problem of this approach is narrow bandwidth and large footprint. The other approach is end-fire coupling which can convert light from dielectric waveguide into MIM structure [9]. Some coupers or mode converters have been investigated under this scheme [10]–[14]. Among them, the taper-funnel (silicon taper and metal funnel) structure is most widely used. Its advantage is compact, broadband and easy to design, but there is always a trade-off between the metallic loss of metal funnel and the reflection loss of silicon taper [9]. Here we propose a mode converter based on a slot-slot coupling scheme, adding a silicon strip-slot mode converter before the conventional taper-funnel (TF) structure, in order to improve the mode and effective index matching. Besides, to overcome the limitation caused by the trade-off mentioned above, we also demonstrate a reversed taper-funnel structure which can avoid metallic propagation and absorption loss during mode conversion.

II. Design

A. MIM Mode Analysis and Propagation Loss

MIM structure in Fig. 1 (a) is essentially a slot waveguide, and its mode is highly confined in the slot region, especially on the metal-dielectric interfaces, which is similar to that of a dielectric slot waveguide, shown in Fig. 1 (b). While for the fundamental transverse electric (TE) mode (the electric field is parallel to the substrate) of a silicon strip waveguide in Fig. 1 (c), the highest field intensity is in the middle of the slot. There is little similarity to the abrupt confinement of the slot waveguides. Fig. 1 (d) illustrates the electric field profile (|Ex|) of three modes with slot width fixed at 80 nm. The mode overlap between two slot waveguides is much larger than that between slot and strip waveguides. The above 2D cross section modes are simulated by finite-difference time-domain (FDTD) method. Dielectric strip-slot mode converters have already been deeply investigated and

Manuscript received December 23, 2015; revised February 16, 2016; accepted February 16, 2016. Date of publication February 28, 2016; date of current version April 11, 2016. This work is supported by the Innovation and Technology Fund project ITS/097/14.

The authors are with the Department of Electronic Engineering, Chinese University of Hong Kong, Shatin, Hong Kong (e-mail: bqzhu@ee.cuhk.edu.hk; hktsang@ee.cuhk.edu.hk).

Color versions of one or more of the figures in this paper are available online at http://ieeexplore.ieee.org.

Digital Object Identifier 10.1109/JLT.2016.2535490

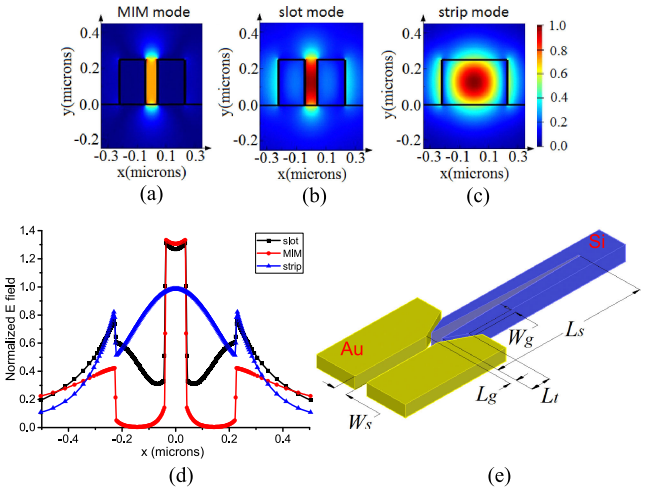

Fig. 1. (a)-(c) Electric field distributions of TE modes for MIM structure, dielectric slot and strip waveguides, respectively. Slot width is fixed at 80 nm. (d) The comparison of electric field profile among the above three modes. (e) Schematic of the ST structure.

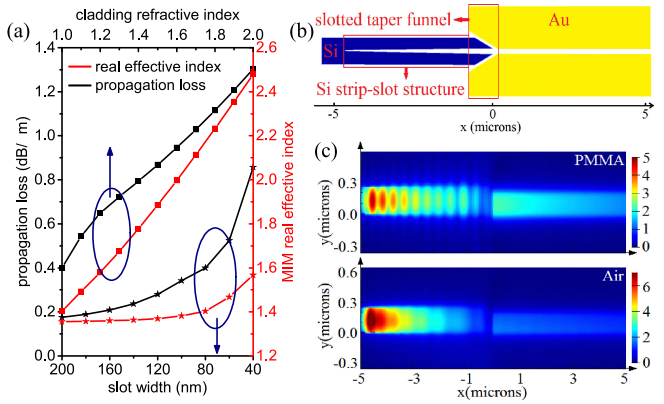

Fig. 2. (a) Real (Red line) and imaginary (black line) parts of MIM mode index vs. slot width under air cladding and mode index vs. cladding material index with slot width fixed at 80 nm. (b) Schematic of the ST structure. (c) Lateral views of electric field distribution for ST structure under PMMA and air cladding, respectively.

widely used [15]–[17], and those well designed and made couplers can experimentally obtain less than 0.1 dB/facet coupling loss. Here, we use a simple Y-branch coupler to achieve the strip-slot mode conversion.

We propose a slot-taper (ST) structure which combines a Y-branch Si strip-slot mode converter with a slotted taper-funnel structure, as shown in Fig. 1 (e). The silicon strip waveguide is 230 nm in height and 450 nm in width sitting on a SiO_2 substrate. Gold is chosen to be the metal and its thickness is 180 nm. We design the slot-taper (ST) structure with the slotted taper length, $L_t = 0.5$ μm, the slot length, $L_s = 4.6$ μm, the gap length, $L_g = 100$ nm, the gap width between silicon and metal, $W_g = 35$ nm, and the MIM slot width, $W_s = 80$ nm. The refractive index of PMMA is set to be 1.489 in simulation. Other materials are all wavelength dependent and their refractive indices are taken from the simulation material database. The 3D structure is simulated by finite-difference time-domain (FDTD) method, and both propagation loss and coupling loss can be calculated from the simulation results. Here, the mode propagation loss is derived as

$$loss(x) = -20 \times log\left(e^{-2\pi\kappa x/\lambda}\right) = (40\pi\kappa x/\lambda) \times log(e) \tag{1}$$

where κ is the imaginary part of MIM mode index and λ is the working wavelength. When air acts as cladding material which is also filled into the slot region, the propagation loss of MIM waveguide is 0.4 dB/μm at 1640 nm. While the cladding material changes to PMMA whose refractive index is very similar to the substrate, the propagation loss increases to 0.86 dB/μm. Fig. 2 (a) illustrates that with the increase of refractive index of the cladding material, both real and imaginary parts of MIM mode index increase as well. This verifies the coexistence of high confinement and high loss in SPP structures. The same trend can also be found when narrowing the slot width, shown in Fig. 2 (a).

B. Coupling Loss Analysis

From simulation, the coupling loss of ST structure is 2.13 dB/coupler under PMMA cladding, and 4.78 dB/coupler under air cladding. When the MIM waveguide is longer than 13 μm, the insertion loss of the whole SPP structure under PMMA cladding will have more loss than the air cladding case. In order to analyze the performance of ST structure, we divide it into two parts as shown in Fig. 2 (b), namely, the Si strip-slot region and the slotted taper-funnel region. Lateral views of the electric field distribution under different claddings are shown in Fig. 2 (c). Because of the better index matching between PMMA and substrate, the mode along y direction is almost symmetric and thus its confinement is higher. The loss induced by Si strip-slot structure can be as low as 0.16 dB under PMMA cladding, while it increases to 0.9 dB in the air cladding case. Mode symmetry in y direction is an important reason for improving the coupling efficiency in PMMA cladding case [11].

Because the loss from Si strip-slot region only contributes a small part, the slotted taper-funnel structure actually dominates the coupling loss. The existence of the slot can efficiently lower the effective mode index, which thus becomes better matched with the MIM mode, so that the reflection is smaller than coupling to a conventional Si taper. Fig. 3 shows the evolution of real effective mode indices and mode cross sections during mode conversion in the taper-funnel region with different coupling strategies. The main picture and upper right corner inset show the PMMA cladding and the air cladding cases respectively, and they have a very similar trend. Taking the PMMA cladding case as an example, the mode index difference between Si strip waveguide and MIM structure is as high as 0.6, so the conventional taper-funnel structure has to be long enough in order to reduce the reflection and radiation loss induced by mode index mismatch. On the other hand, as long as the field touches the metal funnel, the hybrid mode introduces loss, which means we have to keep the taper-funnel structure as short as possible considering the propagation and absorption loss induced by metal. There is always a trade-off between reflection loss and

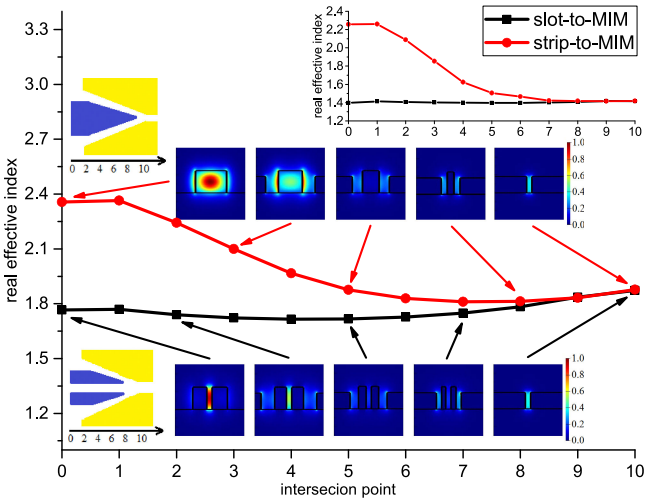

Fig. 3. Mode index changing and mode distribution evolution in taper-funnel region are illustrated. Red line for strip taper-funnel structure, and black line for slotted taper-funnel structure. Schematics for both structures are shown in the inset. The main graph demonstrates the PMMA cladding case, and the upper right corner inset shows the air cladding case.

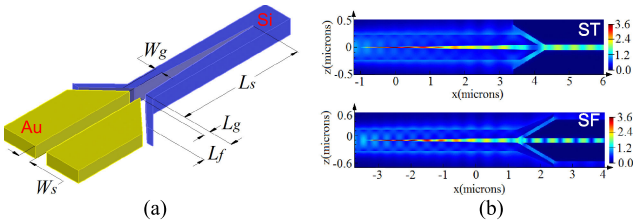

Fig. 4. (a) Schematic of the SF structure. (b) Top views of the mode conversion in ST structure and SF structure, respectively.

propagation loss in conventional TF structure [9], [11], [13]. In comparison, due to the index difference between Si slot waveguide and MIM structure is as low as 0.1, the mode evolution is much smoother than the former, so that we can design the slotted taper-funnel region as short as possible to reduce the metallic propagation loss without considering too much about the reflection. In both simulation and experiment, we choose 500 nm as the slotted taper length in ST structure.

C. Slot-Funnel Structure

We design another mode converter named slot-funnel (SF) structure schematically shown in Fig. 4 (a). It's a reversed taper-funnel structure which depicts a Si funnel and slotted metal tapers. This slot-funnel structure is designed with the funnel length, $L_f = 0.8$ μm, the slot length, $L_s = 4.6$ μm, the gap length, $L_g = 100$ nm, the gap width between silicon and metal, $W_g = 35$ nm, and the MIM slot width, $W_s = 80$ nm. For slot width fixed at 80 nm, the coupling loss of SF structure is 3.49 dB/coupler at 1640 nm. The point here is to avoid introducing excess metallic loss during mode conversion, so the coupling efficiency limited by the trade-off mentioned above can be improved to some extent. Fig. 4 (b) shows the top views of the ST and SF structures during mode conversion. The

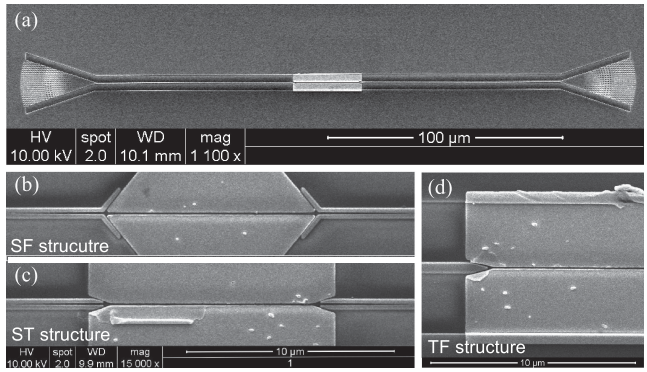

Fig. 5. (a) SEM picture of the whole device including MIM structure, input/output mode converters, Si strip waveguides and subwavelength grating couplers. (b)-(d) Zoom in SEM pictures for SF, ST and conventional TF structures, respectively. The slot widths are all fixed at 80 nm.

operational principle of ST and TF structures is to squeeze the field from the dielectric taper into the metal funnel and gradually narrow it to the MIM waveguide. The metal funnel here is used to form the MIM mode and introduces propagation and absorption loss as well, so the metal surface quality in the mode conversion region really matters a lot in ST and TF structures. In comparison, the SF structure only introduces a small loss in the gaps between metal and Si. Most field in the Si slot directly converts into the subwavelength-confined MIM structure based on the slot-slot coupling scheme. In this case, the effect of metal during mode conversion is minimized, so the metallic loss will decrease and the coupling efficiency will rely less on the metal surface quality.

III. Fabrication

Our devices were implemented on a 230 nm thick silicon-on-insulator (SOI) wafer with 3 μm thick buried oxide. Two steps of electron-beam lithography (EBL) are applied. For the first EBL step, ZEP520 is used as the resist. In this step, subwavelength grating couplers [18], [19], Si strip waveguides and mode converters are created after the deep reactive-ion etching (DRIE). During the second EBL step, bilayer PMMA (lower layer PMMA 495 and upper layer PMMA 950) is applied. Then, metal windows are opened on the resist under very careful alignment with the former silicon structures. 10 nm thick Cr and 170 nm thick Au were deposited onto the chip using sputtering machine and followed by metal lift-off. The last step is spinning coating a thin film of PMMA as the top cladding layer in order to match the refractive index of the buried oxide.

The scanning electron microscope (SEM) picture before spinning coating is shown in Fig. 5 (a). The slot width of MIM waveguide is 80 nm. Three different mode converters, namely SF, ST and TF, are fabricated on the same chip for comparison. Fig. 5 (b)-(d) shows the zoom in SEM images of the three structures. The TF structure is designed in a typical way which tapers a 450 nm width silicon waveguide down to a 60 nm width silicon tip in 800 nm length, as shown in Fig. 5 (d). Besides, MIM waveguides with the same mode converter but different

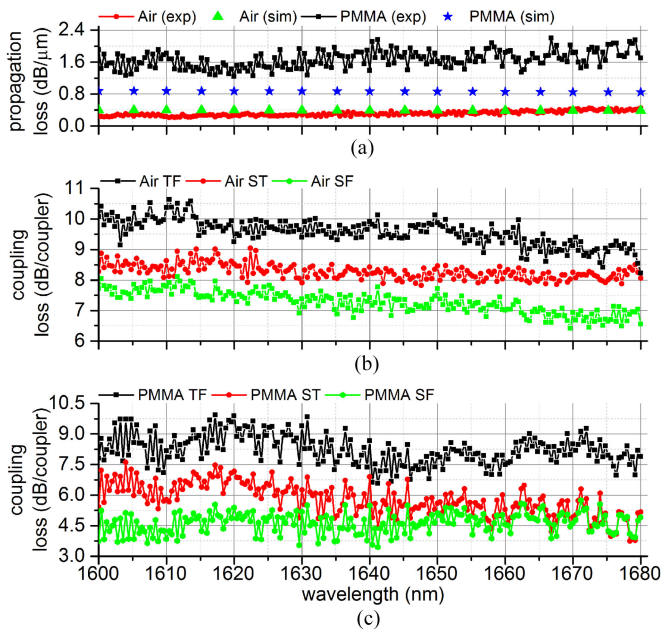

Fig. 6. (a) Simulation and experiment propagation loss spectra of 80-nm-wide MIM waveguide under both claddings. (b)-(c) Coupling loss spectra of three mode converters under air cladding and PMMA cladding, respectively.

lengths (5 μm, 10 μm and 20 μm) are fabricated in order to calculate the propagation loss and the coupling loss of each kind. A reference silicon strip waveguide without any SPP structure is also fabricated on the same chip for normalization of the loss caused by MIM waveguide and input/output mode converters. Experimentally, we couple TE polarized light in and out using a pair of silicon subwavelength grating coupler and measure the transmitted power by a near-infrared power meter.

IV. Experimental Results and Discussions

A. MIM Slot Fixed at 80 nm

We design the MIM slot width to be 80 nm for the following two reasons. First, 80 nm MIM is the narrowest device which we can successfully fabricate. When the slot is 60 nm or less, the 60 nm wide resist structure used to define the MIM waveguide by lift-off, meanders from a straight line and causes large propagation loss. Second, if we want to take good advantage of the field enhancement in MIM waveguide and make it more attractive than the dielectric slot waveguide, slot width less than 100 nm is needed. Dielectric slot width around 100 nm with little loss has been deeply investigated and experimentally realized [20], [21]. After calculation, the propagation loss and coupling loss of our devices are shown in Fig. 6. The spectra are almost wavelength independent and without any apparent resonance. The peak coupling wavelength of our subwavelength grating coupler locates at 1640 nm, so the spectrum range is chosen from 1600 nm to 1680 nm wavelength. In Fig. 6 (a), the propagation loss of the 80-nm-wide MIM waveguide is 0.4 dB/μm under air cladding and 1.8 dB/μm under PMMA cladding at 1640 nm, which matches the simulation outcome well, especially for the air cladding case. The reason for the discrepancy in PMMA cladding case, we believe, is the simulation does not include the material and scattering loss of PMMA.

The coupling loss for each mode converter is also calculated and compared. Fig. 6 (b)-(c) illustrate the coupling loss spectra of the three structures under air and PMMA claddings, respectively. In the air cladding case, the coupling loss of ST structure is 1.5 dB less than TF structure, but 1 dB higher than SF structure at 1640 nm wavelength. In the PMMA cladding case, the coupling loss of ST structure is 2.25 dB less than TF structure, but 1.2 dB higher than SF structure. The graphs show both ST and SF structures have a higher coupling efficiency than the conventional TF structure. Moreover, the SF structure achieves at least 15% additional efficiency compared to the ST structure in both cladding cases. The lowest coupling loss for a fixed 80-nm-wide MIM at 1640 nm is 4 dB/coupler obtained by SF structure under PMMA cladding, and the corresponding propagation loss is 1.8 dB/μm. In comparison, the experimental coupling loss in paper [22], which also applies the slot-slot mode conversion concept and 80 nm MIM slot width, is lower but at cost of much higher propagation loss because of the quasi-MIM waveguide (three walls of its mode touch the metal). Therefore, our designs are supposed to achieve better performance in longer MIM waveguides. For integrated modulator and sensor applications, long MIM waveguide is useful for the device efficiency.

Compared to ST structure, the discrepancy between experiment and simulation results of SF structure is smaller. For ST structure, the silicon slot mode converts to MIM mode by two coupling approaches. First, the field confined in the slot region converts to MIM mode based on slot-slot strategy, which is the only coupling approach appearing in SF structure. Metal is not involved in the forming of MIM mode in this approach. Second, the remaining field that locates in the outside walls of Si tapers is confined and guided into MIM waveguide by the metal funnel. As mentioned before, the metal funnel also introduces metallic loss. In experiment, this coupling process is very sensitive to the quality of the metal surface which cannot be controlled easily in the fabrication. If Au surface of the funnel region is not smooth enough or even not a vertical surface, which often occurs after the metal lift-off, the second coupling approach will reduce rather than improve the coupling efficiency. The problem appears and matters more in conventional TF structure, because it is the only approach involved during its mode conversion. On the other hand, although the potential coupling efficiency of SF structure is not the highest, its coupling approach does not depend as much on the quality of metal surface. As a result, the experimental performance of SF structure is easier to match the simulation result and more predictable.

B. MIM Slot Fixed at 200 nm

In previous experimental works, the MIM slot widths most range from 150 nm to 250 nm, because it is easier to fabricate compared to slot width under 100 nm. In order to verify the high coupling efficiency of our design in this range, we fabricate another group of ST structure with 200-nm-wide MIM slot whose design details are mentioned in [23]. In Fig. 7 (c), because of the wide MIM slot, the propagation loss under PMMA

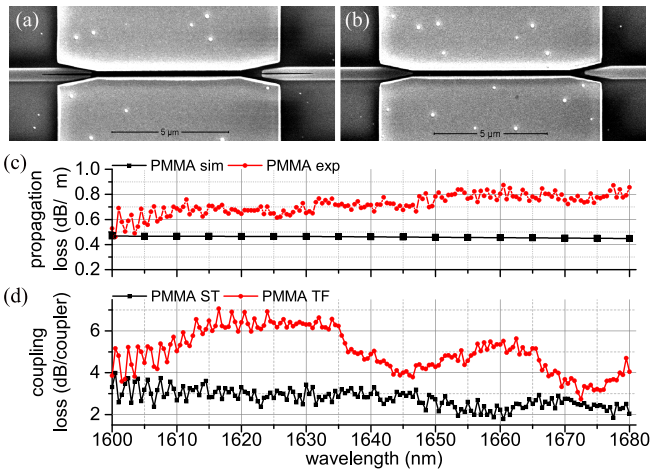

Fig. 7. (a)-(b) SEM pictures of ST and TF structures with 200-nm-wide slot. (c) Simulation and experiment propagation loss spectra of 200-nm-wide MIM waveguide under PMMA cladding. (d) Coupling loss spectra of ST and TF structures.

cladding decreases to a relatively low level of 0.7 dB/μm at 1640 nm as expected, which still keeps good consistency with the simulation result. The MIM propagation loss is comparable to the former experimental results [9], [12] under similar conditions. Next thing is to check the coupling loss. In Fig. 7 (d), the coupling loss of ST structure reaches 3 dB/coupler and is 1.5 dB lower than that of the conventional TF structure at 1640 nm. Besides, there is obvious oscillation in TF structure's spectrum, but not in ST structure's. The reason for the oscillation, we believe, is the horizontal misalignment along the propagation direction between the MIM structure and the silicon counterpart, clearly shown in Fig. 7 (a)-(b). The misalignment can cause large mode index mismatch and form a weak F-P cavity between in and out mode converters. According to our MIM waveguide length and effective mode index (L $\sim$ 17 μm, n_{eff} $\sim$ 1.67 μm), the free spectral range (FSR) of the F-P cavity is $\sim$45 nm which well matches the oscillation period in the spectrum in Fig. 7 (d). As expected, the ST structure is more tolerant to the fabrication deviation, because the slotted taper structure has superiority in matching the effective mode index of MIM waveguide. To our knowledge, our TF structure possesses the same or even higher coupling efficiency compared to the previous works under very similar conditions, so the even higher efficiency achieved by ST structure is robustly realized.

C. Discussions

According to Figs. 6 (a) and 7(c), the experimental propagation loss increases slowly with wavelength, while the simulation results do not show the same trend. In practical fabrication, the metal surface roughness is typically in the order of few nanometers and is comparable to the skin depth of gold in the near-infrared wavelength. With the increase of wavelength, the skin depth also increases, so that more field will locate in the metal side and touch the rough surface, which causes larger scattering loss. But the simulation does not include surface roughness and scattering loss. In general, the reasons for the discrepancy between simulation and experiment results can be classified into four categories: material and scattering loss of PMMA and gold, not perfect metal surface and surface roughness, misalignment between gold structure and Si counterparts, and finite small tips with rounded corners.

V. Conclusion

In conclusion, we propose two designs of high efficiency mode converters, namely ST structure and SF structure, to convert mode from Si strip waveguide to MIM waveguide based on the slot-slot coupling scheme. Simulation indicates the dielectric slot waveguide and MIM structure have large mode overlap and very similar effective indices. For 80-nm-wide MIM slot, the best coupling efficiency experimentally achieved by SF structure is 4 dB/coupler and the corresponding propagation loss is 1.8 dB/μm at 1640 nm wavelength. For MIM slot fixed at 200 nm, the best performance of the ST structure is 3 dB/coupler with only 0.7 dB/μm propagation loss at 1640 nm. It should be noted that it is still very difficult to fabricate plasmonic photonic devices in practice because of their small sizes and the accurate alignment needed in double layer EBL. It is proved that ST structure has high tolerance to the fabrication misalignment and SF structure depends less on the fabricated metal surface quality. The mode converters introduced in this paper provide a good coupling scheme between the plasmonic devices and the integrated silicon photonic platform. The coupling structures may find use in advanced passive and active plasmonic photonic circuits [24], [25], especially in ultracompact high-speed optical modulators [5], [26] integrated with novel electrooptic polymers that can be directly filled into the MIM slot, which shows promising prospects.

Acknowledgment

The author wants to acknowledge the support from Innovation and Technology Fund project ITS/097/14. The authors would like to thank Prof. Zhenzhou Cheng for designing the subwavelength grating couplers, Prof. Xiankai Sun and Dr. Jinjin Liu for the kindly help and suggestion in fabrication.

References

[1] D. K. Gramotnev and S. I. Bozhevolnyi, "Plasmonics beyond the diffraction limit," *Nature Photon.*, vol. 4, no. 2, pp. 83–91, Feb. 2010.
[2] J. Dionne, L. Sweatlock, H. Atwater, and A. Polman, "Plasmon slot waveguides: Towards chip-scale propagation with subwavelength-scale localization," *Phys. Rev. B*, vol. 73, no. 3, p. 035407, Jan. 2006.
[3] G. Veronis and S. Fan, "Modes of subwavelength plasmonic slot waveguides," *J. Lightw. Technol.*, vol. 25, no. 9, pp. 2511–2521, Sep. 2007.
[4] S. A. Maier, *Plasmonics: Fundamentals and Applications*. New York, NY, USA: Springer, 2007.
[5] A. Melikyan, L. Alloatti, A. Muslija, D. Hillerkuss, P. Schindler, J. Li, R. Palmer, D. Korn, S. Muehlbrandt, D. Van Thourhout et al. *et al.*, "High-speed plasmonic phase modulators," *Nature Photon.*, vol. 8, no. 3, pp. 229–233, Feb. 2014.
[6] J. A. Schuller, E. S. Barnard, W. Cai, Y. C. Jun, J. S. White, and M. L. Brongersma, "Plasmonics for extreme light concentration and manipulation," *Nature Mater.*, vol. 9, no. 3, pp. 193–204, Mar. 2010.
[7] R. H. Ritchie, E. T. Arakawa, J. J. Cowan, and R. N. Hamm, "Surface-plasmon resonance effect in grating diffraction," *Phys. Rev. Lett.*, vol. 21, pp. 1530–1533, Nov. 1968.

[8] W. D. Wilson, "Analyzing biomolecular interactions," *Science*, vol. 295, no. 5562, pp. 2103–2105, Mar. 2002.
[9] L. Chen, J. Shakya, and M. Lipson, "Subwavelength confinement in an integrated metal slot waveguide on silicon," *Opt. Lett.*, vol. 31, no. 14, pp. 2133–2135, Jul. 2006.
[10] Z. Han, A. Elezzabi, and V. Van, "Experimental realization of subwavelength plasmonic slot waveguides on a silicon platform," *Opt. Lett.*, vol. 35, no. 4, pp. 502–504, Feb. 2010.
[11] C.-T. Chen, X. Xu, A. Hosseini, Z. Pan, H. Subbaraman, X. Zhang, and R. T. Chen, "Design of highly efficient hybrid si-au taper for dielectric strip waveguide to plasmonic slot waveguide mode converter," *J. Lightw. Technol.*, vol. 33, no. 2, pp. 535–540, Jan. 2015.
[12] J. Tian, S. Yu, W. Yan, and M. Qiu, "Broadband high-efficiency surface-plasmon-polariton coupler with silicon-metal interface," *Appl. Phys. Lett.*, vol. 95, no. 1, p. 013504, 2009.
[13] N.-N. Feng and L. Dal Negro, "Plasmon mode transformation in modulated-index metal-dielectric slot waveguides," *Opt. Lett.*, vol. 32, no. 21, pp. 3086–3088, 2007.
[14] H. Choo, M.-K. Kim, M. Staffaroni, T. J. Seok, J. Bokor, S. Cabrini, P. J. Schuck, M. C. Wu, and E. Yablonovitch, "Nanofocusing in a metal-insulator-metal gap plasmon waveguide with a three-dimensional linear taper," *Nature Photon.*, vol. 6, no. 12, pp. 838–844, Nov. 2012.
[15] Q. Deng, L. Liu, X. Li, and Z. Zhou, "Strip-slot waveguide mode converter based on symmetric multimode interference," *Opt. Lett.*, vol. 39, no. 19, pp. 5665–5668, Oct. 2014.
[16] Z. Wang, N. Zhu, Y. Tang, L. Wosinski, D. Dai, and S. He, "Ultracompact low-loss coupler between strip and slot waveguides," *Opt. Lett.*, vol. 34, no. 10, pp. 1498–1500, May 2009.
[17] R. Palmer, L. Alloatti, D. Korn, W. Heni, P. C. Schindler, J. Bolten, M. Karl, M. Waldow, T. Wahlbrink, W. Freude, C. Koos, and J. Leuthold "Low-loss silicon strip-to-slot mode converters," *IEEE Photonics J.*, vol. 5, no. 1, p. 2200409, Jan. 2013.
[18] X. Chen, K. Xu, Z. Cheng, C. K. Fung, and H. K. Tsang, "Wideband subwavelength gratings for coupling between silicon-on-insulator waveguides and optical fibers," *Opt. Lett.*, vol. 37, no. 17, pp. 3483–3485, 2012.
[19] Z. Cheng, X. Chen, C. Y. Wong, K. Xu, and H. K. Tsang, "Apodized focusing subwavelength grating couplers for suspended membrane waveguides," *Appl. Phys. Lett.*, vol. 101, no. 10, p. 101104, 2012.
[20] Q. Xu, V. R. Almeida, R. R. Panepucci, and M. Lipson, "Experimental demonstration of guiding and confining light in nanometer-size low-refractive-index material," *Opt. Lett.*, vol. 29, no. 14, pp. 1626–1628, Jul. 2004.
[21] R. Ding, T. Baehr-Jones, W.-J. Kim, B. Boyko, R. Bojko, A. Spott, A. Pomerene, C. Hill, W. Reinhardt, and M. Hochberg, "Low-loss asymmetric strip-loaded slot waveguides in silicon-on-insulator," *Appl. Phys. Lett.*, vol. 98, no. 23, p. 233303, Jun. 2011.
[22] R. Yang, R. A. Wahsheh, Z. Lu, and M. A. Abushagur, "Efficient light coupling between dielectric slot waveguide and plasmonic slot waveguide," *Opt. Lett.*, vol. 35, no. 5, pp. 649–651, Mar. 2010.
[23] B. Q. Zhu and H. K. Tsang, "A new design for coupling light between silicon strip waveguide and plasmonic slot waveguide," presented at the *Photonic West Proc.*, San Francisco, CA, USA, 2016.
[24] S. I. Bozhevolnyi, V. S. Volkov, E. Devaux, J.-Y. Laluet, and T. W. Ebbesen, "Channel plasmon subwavelength waveguide components including interferometers and ring resonators," *Nature*, vol. 440, no. 7083, pp. 508–511, Mar. 2006.
[25] M. Xu, F. Li, T. Wang, J. Wu, L. Lu, L. Zhou, and Y. Su, "Design of an electro-optic modulator based on a silicon-plasmonic hybrid phase shifter," *J. Lightw. Technol.*, vol. 31, no. 8, pp. 1170–1177, Apr. 2013.
[26] C. Haffner, W. Heni, Y. Fedoryshyn, J. Niegemann, A. Melikyan, D. Elder, B. Baeuerle, Y. Salamin, A. Josten, U. Koch et al. *et al.*, "All-plasmonic mach–zehnder modulator enabling optical high-speed communication at the microscale," *Nature Photon.*, vol. 9, no. 8, pp. 525–528, Jul. 2015.

Bing Qing Zhu received the B.Eng. degree from Zhejiang University, Hangzhou, China, in 2012. She is currently working toward the Ph.D. degree in the Department of Electronic Engineering, Chinese University of Hong Kong, Shatin, Hong Kong. Her research interests include silicon photonics, plasmonics, and polymer hybrid integrated nanophotonic devices.

Hon Ki Tsang (M'91–SM'04) received the B.A. and Ph.D. degrees from the University of Cambridge, Cambridge, U.K., in 1987 and 1991, respectively. He is currently a Professor and the Chairman of the Department of Electronic Engineering, Chinese University of Hong Kong, Shatin, Hong Kong. His research interests include silicon photonics and two-dimensional photonic materials.